Evaluation of Wind Vectors Observed by QuikSCAT/SeaWinds Using Ocean Buoy Data

NAOTO EBUCHI*

Center for Atmospheric and Oceanic Studies, Graduate School of Science, Tohoku University, Aoba, Sendai, Japan

HANS C. GRABER

Rosenstiel School of Marine and Atmospheric Studies, University of Miami, Miami, Florida

MICHAEL J. CARUSO

Woods Hole Oceanographic Institution, Woods Hole, Massachusetts

(Manuscript received 23 July 2001, in final form 15 April 2002)

ABSTRACT

Wind vectors observed by the QuikSCAT/SeaWinds satellite mission are validated by comparing with wind and wave data from ocean buoys. Effects of oceanographic and atmospheric environment on scatterometer measurements are also assessed using the buoy data. Three versions of QuikSCAT/SeaWinds wind data were collocated with buoy observations operated by the National Data Buoy Center (NDBC), Tropical Atmosphere Ocean (TAO), and Pilot Research Moored Array in the Tropical Atlantic (PIRATA) projects, and the Japan Meteorological Agency (JMA). Only buoys located offshore and in deep water were analyzed. The temporal and spatial differences between the QuikSCAT/SeaWinds and buoy observations were limited to less than 30 min and 25 km. The buoy wind speeds were converted to equivalent neutral winds at a height of 10 m above the sea surface. The comparisons show that the wind speeds and directions observed by QuikSCAT/SeaWinds agree well with the buoy data. The root-mean-squared differences of the wind speed and direction for the standard wind data products are 1.01 m s^{-1} and 23°, respectively, while no significant dependencies on the wind speed or cross-track cell location are discernible. In addition, the dependencies of wind speed residuals on oceanographic and atmospheric parameters observed by buoys are examined using the collocated data. A weak positive correlation of the wind speed residuals with the significant wave height is found, while dependencies on the sea surface temperature or atmospheric stability are not physically significant.

1. Introduction

QuikSCAT (QSCAT) was launched by the National Aeronautics and Space Administration (NASA) on 19 June 1999, as a ''quick recovery'' mission to fill the gap created by the loss of data from the NASA Scatterometer (NSCAT), when the Japanese Advanced Earth Observation Satellite (*ADEOS*) lost power in June 1997 (JPL 2001). The QSCAT satellite was launched into a sun-synchronous, 98.6° inclination, 803 km, circular orbit with a local equator crossing time at the ascending node of 6:00 A.M. ± 30 min. The recurrent and orbital periods of the orbit are 4 days and 101 min, respectively. The mission carries a Ku-band scatterometer named SeaWinds. A similar version of the SeaWinds instrument will also fly on *ADEOS-II* currently scheduled for launch in 2002.

The SeaWinds instrument on the QSCAT satellite is a microwave scatterometer that measures near-surface wind speed and direction under all weather and cloud conditions over the global oceans. It uses a rotating dish antenna with two pencil beams that sweep in a circular pattern at incidence angles of 46° (H-pol) and 52° (V-pol). The antenna radiates microwave pulses at a frequency of 13.4 GHz across broad regions on the earth's surface. The instrument can measure vector winds over a swath of 1800 km with a nominal spatial resolution of 25 km. Daily coverage is about 92% of the global ice-free oceans.

* Current affiliation: Institute of Low Temperature Science, Hokkaido University, Kita-Ku, Sapporo, Japan.

Corresponding author address: Dr. Naoto Ebuchi, Institute of Low Temperature Science, Hokkaido University, Kita 19, Nishi 8, Kita-ku, Sapporo 060-0819, Japan.
E-mail: ebuchi@lowtem.hokudai.ac.jp

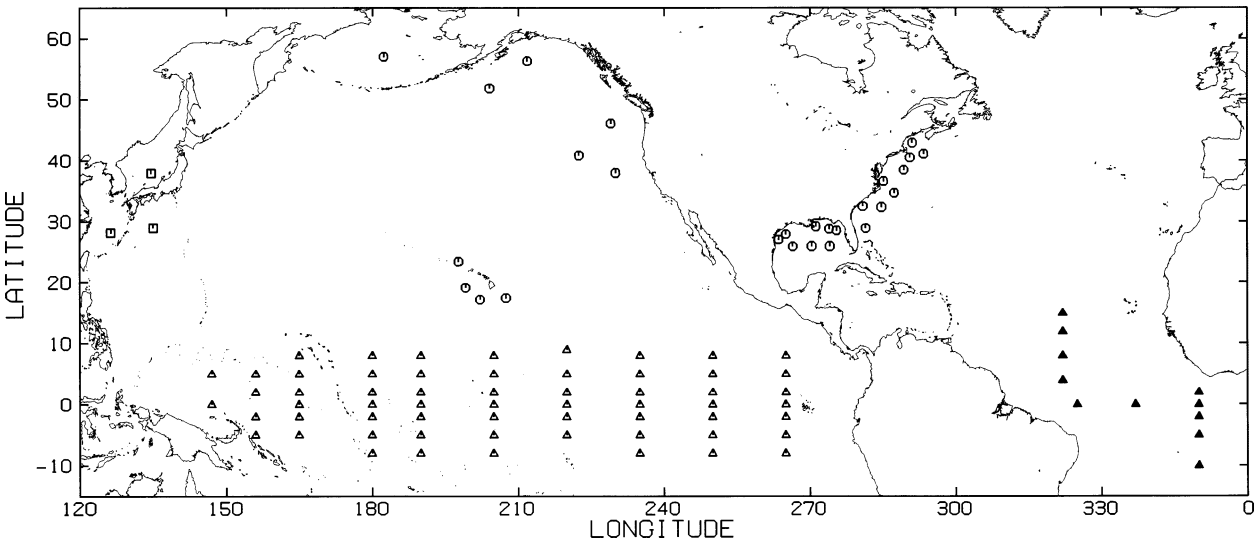

FIG. 1. Location of the NDBC (circles), TAO (open triangles), PIRATA (solid triangles), and JMA (boxes) buoys used in the present study.

Wind vectors observed over the global oceans with high spatial resolution and frequent temporal sampling by spaceborne scatterometers are utilized in various fields of meteorology, oceanography, and climate studies, such as ocean surface waves, wind-driven current systems, and air–sea fluxes of momentum, heat, water vapor, and gasses. Surface wind and stress fields derived from scatterometer observations can be applied to drive ocean circulation models on various scales, and can also be assimilated into regional and global numerical weather prediction models. However, scatterometers do not measure the marine surface wind directly but measure the electromagnetic radiation signal backscattered from the sea surface. Winds are estimated using a Geophysical Model Function (GMF) that relates the backscatter to 10-m neutral equivalent winds. Therefore, validation of the observed wind vectors is necessary to evaluate the quality of the wind data and to assess the error structure.

Numerous validation studies have been carried out by comparing scatterometer-derived winds with in situ observations by buoys and vessels for the Seasat-A Scatterometer (SASS) (e.g., Jones et al., 1982), the Active Microwave Instrument on the European Remote Sensing Satellite (ERS/AMI) (e.g., Bentamy et al. 1994; Quilfen and Bentamy 1994; Ebuchi et al. 1996, Graber et al. 1996), and ADEOS/NSCAT (e.g., Bourassa et al. 1997; Freilich and Dunber 1999; Ebuchi et al. 1998, 1999; Masuko et al. 2000; Dickinson et al. 2001).

In the present study, wind vectors observed by QSCAT/SeaWinds are compared with ocean buoy observations to validate the QSCAT geophysical model function and retrieved wind vectors. The SeaWinds instrument departs from the more traditional and validated fan beams used by the previous scatterometers, such as SASS, NSCAT, and AMI, and uses conical-scan pencil beams. The structure of errors may differ from previous studies due to the new and innovative design of the SeaWinds instrument. To complete this study, the effects of oceanographic and atmospheric parameters on the scatterometry are also assessed by using the buoy data.

2. Data

In the present study, three versions of QSCAT wind data are compared with buoy data. Two of the datasets were produced by the NASA Jet Propulsion Laboratory (JPL) and one was produced by Remote Sensing Systems.

The QuikSCAT Operational Standard Data Products (Level 2.0), which have been processed and distributed by the NASA JPL Physical Oceanography Distributed Active Archive Center (PO.DAAC), contain two outputs of wind data. One is the standard wind data, which have been produced using a Maximum Likelihood Estimator (MLE) (Long and Mendel 1991) and median filter ambiguity removal algorithm (Shaffer 1991) with the Numerical Weather Product (NWP) initialization. The other is enhanced wind data processed using the Direction Interval Retrieval with Thresholded Nudging (DIRTH) algorithm (JPL 2001). Hereafter we abbreviate these data to L2B and DIRTH wind data, respectively.

Both of the wind data have been retrieved with the QSCAT-1 geophysical model function, which was developed based on results of postlaunch calibration/validation activities. The spatial resolution of the data is 25 km, and the reference height of the wind vectors is 10 m above the sea surface. The Multidimensional Histogram rain flagging (Huddleston and Stiles 2000) is applied to indicate the presence of rain. The present analysis included all data flagged for low and high wind speeds, and all other flagged data, such as the rain flag,

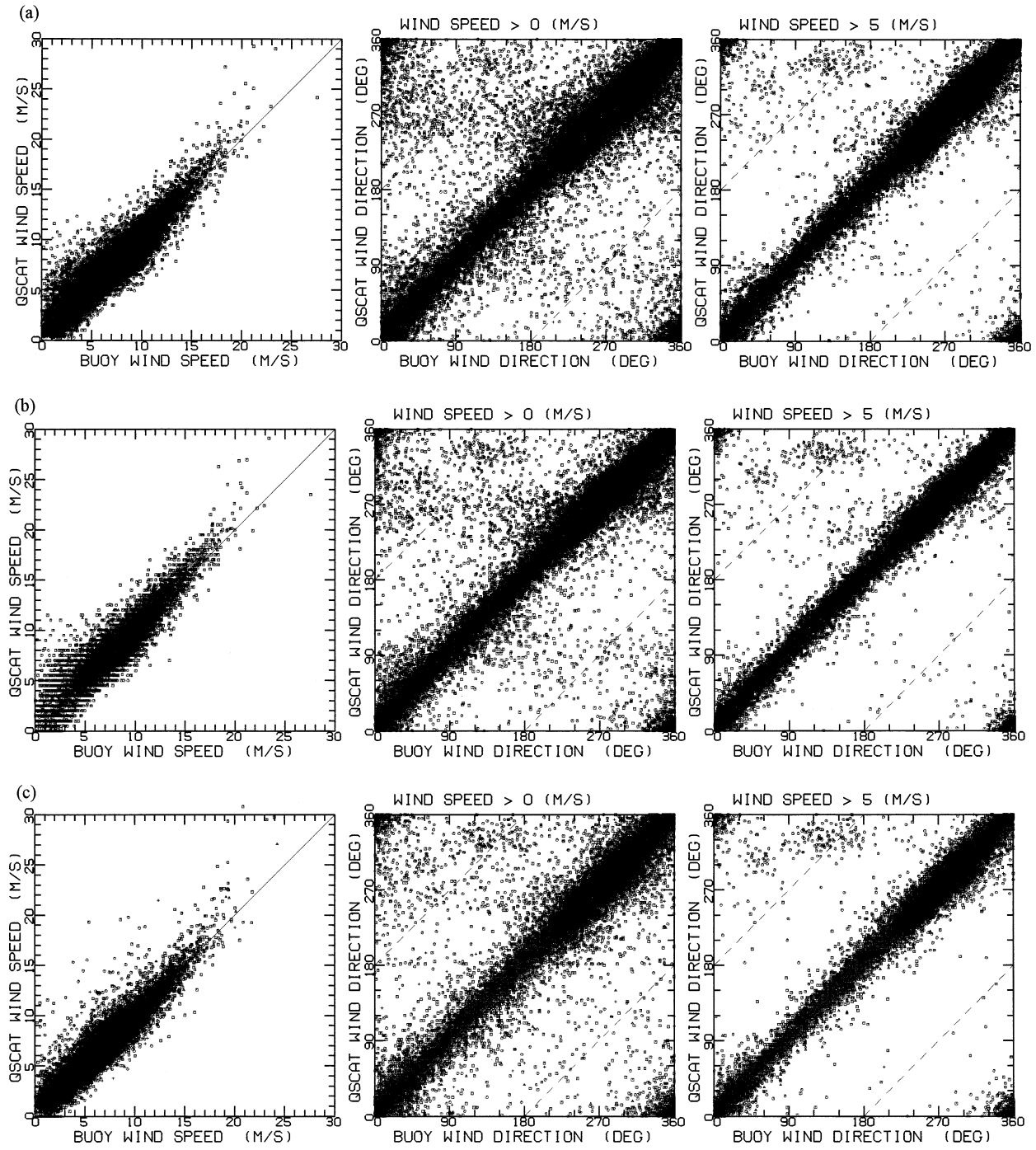

FIG. 2. Comparison of wind speed and direction observed by QSCAT/SeaWinds with data from all the buoys for (a) the L2B, (b) DIRTH, and (c) RSS wind data. Comparison of (left) wind speed, (middle) wind direction for data of all the wind speed ranges, and (right) of wind speed greater than 5 m s^{-1}, respectively.

were discarded. Data observed in a period from 19 July 1999 to 31 December 2000 are used.

In addition to the L2B and DIRTH wind data, we also utilized wind data produced and distributed by the Remote Sensing Systems (version 2). The wind data have been retrieved by their new Ku-2000 model function. In addition to the new geophysical model function, their wind data processing uses contemporaneous microwave radiometer measurements by three Special Sensor Microwave Imagers and the Tropical Rainfall Measuring Mission Microwave Imager for rain flagging and sea ice detection. More details of the wind data are described

TABLE 1. Statistics of the comparisons of QSCAT wind speed and direction with buoy data.

	Number of data	Bias	Rms difference	Correlation coefficient
L2B				
Wind speed (m s^{-1})	48 540	0.02	1.01	0.925
Wind direction (deg.)				
(Buoy wind speed $>$ 0 m s^{-1})	48 519	1.5	29.6	0.948
(Buoy wind speed $>$ 3 m s^{-1})	43 952	1.6	23.3	0.965
(Buoy wind speed $>$ 5 m s^{-1})	35 092	1.7	19.5	0.973
DIRTH				
Wind speed (m s^{-1})	48 540	0.05	1.00	0.927
Wind direction (deg.)				
(Buoy wind speed $>$ 0 m s^{-1})	48 519	1.5	28.3	0.952
(Buoy wind speed $>$ 3 m s^{-1})	44 160	1.5	22.4	0.967
(Buoy wind speed $>$ 5 m s^{-1})	35 619	1.6	18.8	0.975
RSS				
Wind speed (m s^{-1})	34 167	−0.02	1.01	0.925
Wind direction (deg.)				
(Buoy wind speed $>$ 0 m s^{-1})	34 119	1.7	26.5	0.959
(Buoy wind speed $>$ 3 m s^{-1})	31 101	1.7	20.5	0.973
(Buoy wind speed $>$ 5 m s^{-1})	24 992	1.9	18.6	0.977

online at their Web site (http://www.ssmi.com). Hereafter the wind data are abbreviated to RSS wind data.

In order to compare with the QSCAT/SeaWinds wind data, we collected buoy observations from 27 buoys operated by the National Data Buoy Center (NDBC), 60 buoys by the Tropical Atmosphere Ocean (TAO) project, 11 buoys by the Pilot Research Moored Array in the Tropical Atlantic (PIRATA) project, and 3 buoys by the Japan Meteorological Agency (JMA). The buoy locations are shown in Fig. 1. Only the buoys moored offshore and in deep water were selected. Details of the buoys, instruments, and stations were described by Meindl and Hamilton (1992), McPhaden (1995), and WMO/IOC Data Buoy Cooperation Panel (1996), respectively. The PIRATA buoys are identical to the TAO buoys. The wind speed measured by the buoys at various heights above the sea surface was converted to equivalent neutral wind speed at a height of 10 m using a method proposed by Liu and Tang (1996). A direction bias of 6.8° due to firmware and circuitry errors was also corrected in the TAO observations obtained by the buoys deployed before November 2000 (Freitag et al. 2001). The temporal interval of the NDBC and standard TAO buoy observations is 1 h, while that of the JMA buoys is 3 h. New generation TAO buoys record the wind every 10 min.

The QSCAT/SeaWinds data and buoy observations were collocated in time and space. QSCAT wind vector cells closest to the buoy locations in space and the buoy data closest to the QSCAT observations in time were chosen. The temporal difference and spatial separation between the QSCAT and buoy observations were limited to less than 30 min and 25 km, respectively.

3. Results and discussion

a. Comparison of wind speed and direction

Figure 2 shows an example of the comparisons of wind speed and direction observed by QSCAT and the buoys for (a) the L2B, (b) DIRTH, and (c) RSS wind data. In general, the wind speed and direction derived by QSCAT agree well with buoy observations. No systematic biases in the wind speed or direction are discernible. Statistics of the comparisons for the three wind data are summarized in Table 1.

In the comparison of wind speed, the bias is negligibly small, and the rms difference is about 1 m s^{-1}, which is much smaller than the mission requirement of 2 m s^{-1} for all of the three datasets. At very high wind ranges ($>$15 m s^{-1}), the wind speed of the L2B and DIRTH winds is slightly overestimated, and is significantly overestimated for the RSS winds. This trend in the wind speed will be discussed in section 3b. In Fig. 2b, the distribution of data points for the DIRTH wind speeds exhibits horizontal stripes, due to coarse truncation of the DIRTH wind speed.

For wind direction, the rms difference is greater than 25° for the whole wind speed range. Taking data of buoy wind speed higher than 3 m s^{-1}, the rms difference is considerably reduced to about 20°, implying that the accuracy of the QSCAT-derived wind direction at low wind speed range is worse than that at moderate to high wind ranges. The mission requirement for wind direction is 20° in a wind speed range between 3 and 30 m s^{-1}. We may conclude that the mission requirement for the wind direction is also met, if we consider uncertainty in the measurements of wind direction by the buoys and temporal and spatial separations of the observations,

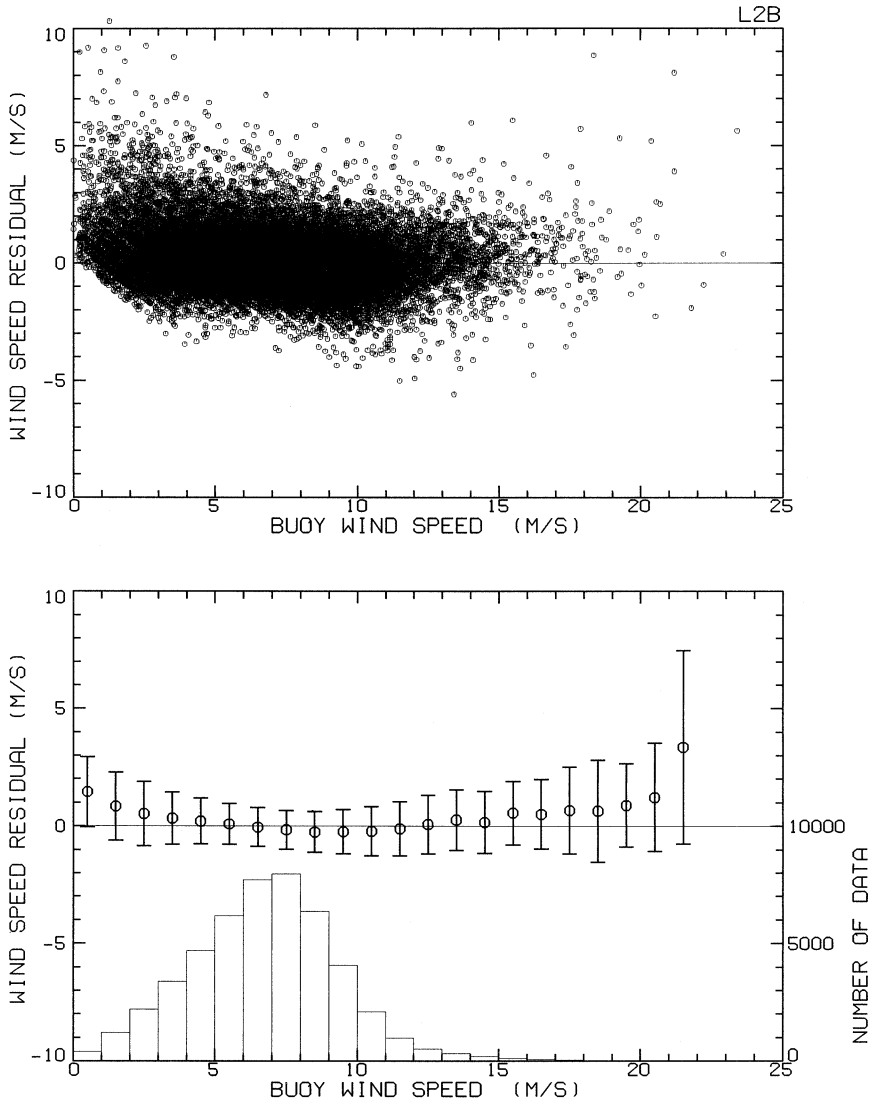

FIG. 3. Dependence of wind speed residual (QSCAT − buoy) on the buoy wind speed for the L2B winds. (upper panel) Scatterplots and (lower panel) numbers of data points, averages, (circles) and standard deviations (vertical lines) calculated in bins of buoy wind speed of 1 m s^{-1}.

which may increase the rms difference of the comparison. The rms difference for the RSS data is smaller than those for the L2B and DIRTH data. However, the number of collocated data points for the same period is smaller for the RSS data, since the rain flagging for the RSS data is more strict than the others.

b. Analysis of residuals

Figure 3 shows dependencies of wind speed residual (QSCAT-buoy) on the buoy wind speed for the L2B winds. The upper panel shows scatterplot, and the lower panel shows the numbers of data, averages, and standard deviations calculated in bins of buoy wind speed of 1 m s^{-1}. The wind speed residual is almost zero and shows no systematic dependence on the buoy wind speed over a wind range from 5 to 15 m s^{-1}. At low wind speeds (<5 m s^{-1}), an artificial positive bias due to asymmetrical distribution of data points about the one-to-one line (Freilich 1997), which does not imply systematic overestimation of the wind speed, is discernible. At very high winds (>15 m s^{-1}), the QSCAT wind speed is slightly higher than the buoy wind speed as seen in Fig. 2. In this wind range, however, the comparison is questionable due to motion of the buoy in high waves, surface layer distortion (Large et al. 1995) and the exclusion of local surface conditions in the GMF. The DIRTH wind speeds (not shown) exhibit the same dependence because the L2B and DIRTH winds are retrieved using the same geophysical model function, QSCAT-1.

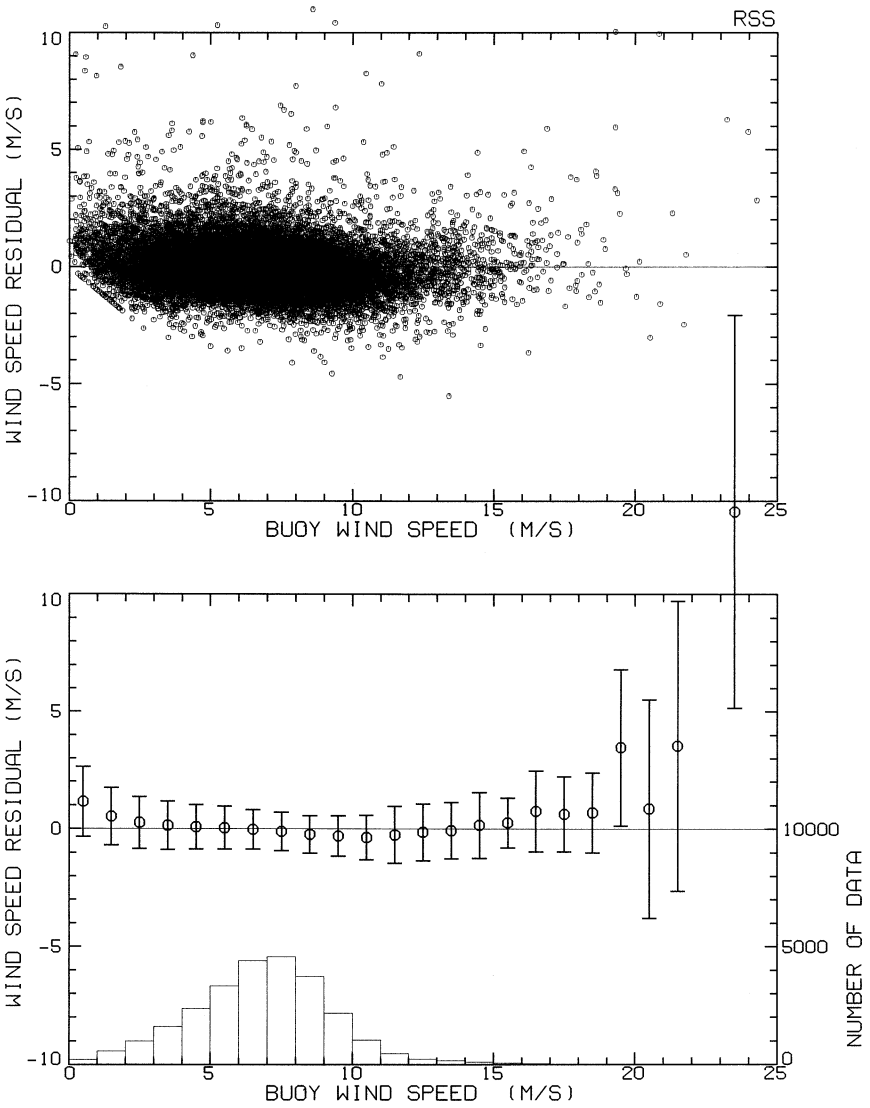

FIG. 4. Same as Fig. 3 except for the RSS wind data.

In Fig. 4, the dependence of the wind speed residual on the buoy wind speed is shown for the RSS data. As also seen in Fig. 2, the RSS data give higher wind speeds compared to the L2B winds at very high wind speeds. In this wind range, as mentioned before, we cannot evaluate the wind speed using the buoy observations. Several efforts to obtain more reliable reference wind data and improve GMF under the extreme wind conditions are now ongoing (e.g., Yueh et al. 2001).

Figure 5 shows dependencies of wind direction residual on the buoy wind speed for the L2B winds. The standard deviation increases at low wind speeds, corresponding to the result in Table 1 and showing that the wind direction at low winds is less accurate. This may be due to the low upwind/crosswind modulation of the microwave backscattering from the sea surface. The ambiguity removal procedure may also be less accurate at low wind speeds, which will be discussed in section 3d. The same trend is found for the DIRTH and RSS winds, though the results are not shown here.

Dependencies of the residuals on cross-track location of wind vector cells, which corresponds to combination of azimuth angles of the scatterometer beams, are shown in Fig. 6 for the L2B wind data. Histograms of data points, binned averages, and standard deviations are also shown in the lower panels. At outer cells (toward cells 1 and 76), the scatterometer beams are aligned to the cross-track directions, and at inner cells (toward cells 38 and 39), they are alined to the spacecraft flight direction. For the wind speed residual in Fig. 6a, the standard deviation slightly increases toward the inner and outer cells, though it is not significant. For the residual of wind direction in Fig. 6b, only the data of buoy wind speed ranging between 3 and 15 m s^{-1} are used to isolate

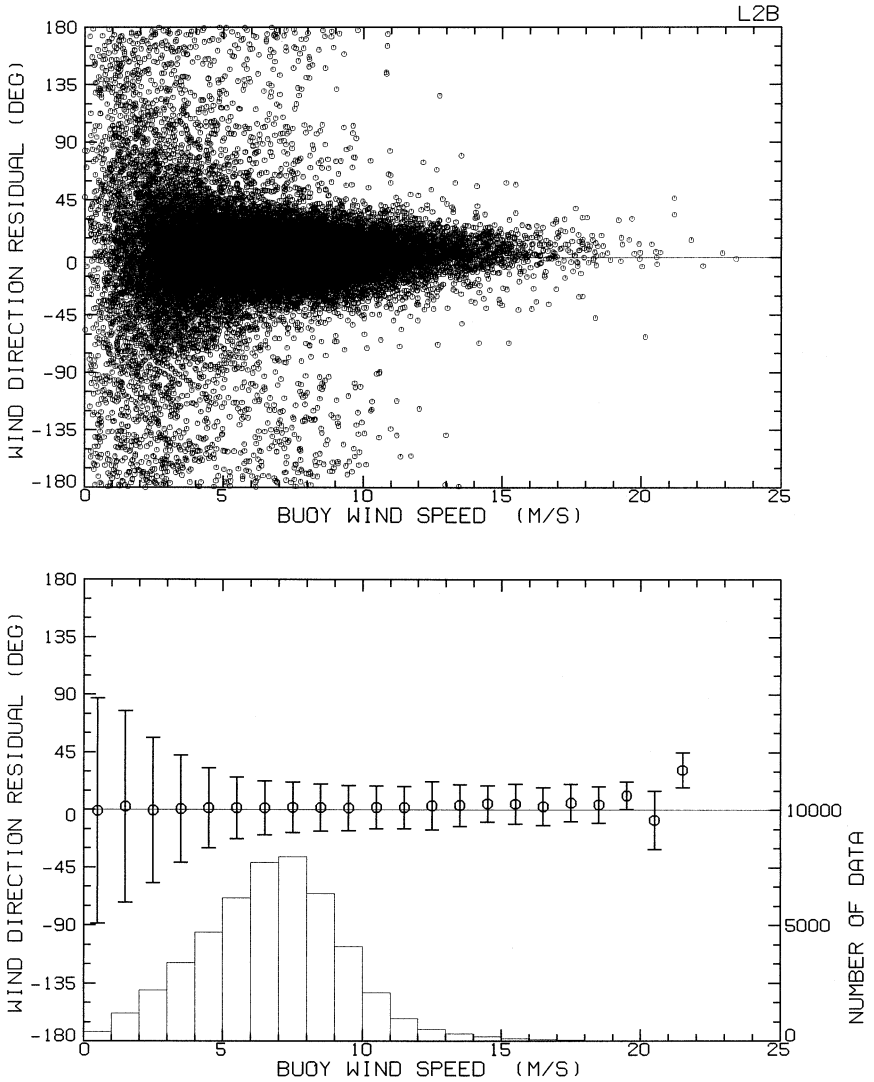

FIG. 5. Dependence of wind direction residual (QSCAT − buoy) on the buoy wind speed for the L2B winds. (upper panel) Scatterplots and (lower panel) numbers of data points, averages (circles), and standard deviations (vertical lines) calculated in bins of buoy wind speed of 1 m s^{-1}.

TABLE 2. Correlation of the wind speed residual (QSCAT − buoy) with the atmospheric and oceanic parameters (buoy wind speed ranging from 9 to 12 m s^{-1}).

Parameter	Number of data	Correlation coefficient	Slope of linear regression line
Sea surface temperature (SST)	7139	−0.152*	−0.023 m s^{-1} $(deg)^{-1}$
Air temperature	7139	−0.167*	−0.023 m s^{-1} $(deg)^{-1}$
Air–sea temperature difference	7139	−0.103*	−0.049 m s^{-1} $(deg)^{-1}$
Specific humidity	3961	0.036	−0.014 m s^{-1} $(gm^{-3})^{-1}$
Bulk Richardson number	7139	−0.101*	−14.53 m s^{-1}
Significant wave height (SWH)	3184	0.211*	0.227 m s^{-1} $(m)^{-1}$
Inverse wave age	3178	−0.151*	−0.7071 m s^{-1}
Buoy wind speed	7139	0.036	0.047 m s^{-1} $(ms^{-1})^{-1}$

* Denotes correlation coefficient higher than 99% confidence limit.

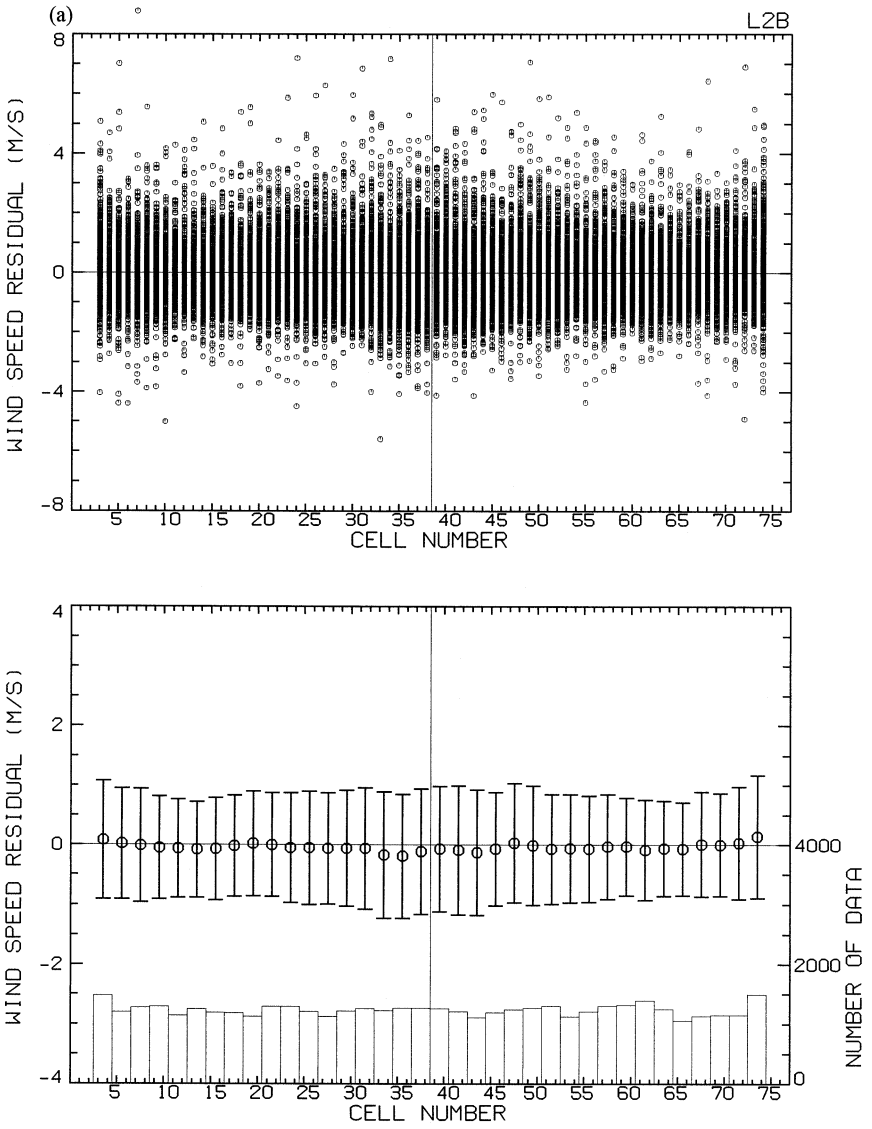

FIG. 6. Dependence of residuals (QSCAT − buoy) of (a) the wind speed and (b) direction on location of the wind vector cells for the L2B winds. (upper panels) Scatterplots and (lower panels) numbers of data points, binned averages (circles), and standard deviations (vertical lines).

the high direction variability shown in Fig. 3. No systematic dependence on the wind vector cell location is discernible. These characteristics are the same for the DIRTH and RSS data, though the results are not shown here.

c. Effects of atmospheric and oceanic environment

In order to assess the influence of the atmospheric and oceanic conditions on the scatterometry, correlations of the wind speed residual with atmospheric and oceanic parameters observed by the buoys were calculated for the L2B winds and shown in Table 2. Only the data of buoy wind speed ranging from 9 to 12 m s^{-1} are used to eliminate a spurious effect of wind speed dependence of the residual. The number of data points differ for each parameter, since the NDBC buoys do not measure the humidity, and the TAO buoys do not measure the wave parameters. In the last line, the correlation of the residual with the buoy wind speed is shown to confirm that the residual has no dependence on the wind speed itself and the obtained correlation is not due to the spurious effect of wind speed dependence of the residual.

The bulk Richardson number, R_i, which represents the stability of the atmospheric boundary layer is estimated according to Toba et al. (1990) as

$$R_i = z_{10} g (T_a - T_w)/(273 + T_a) U_{10N}^2, \qquad (1)$$

where z_{10} is a height of 10 m, g is the acceleration of

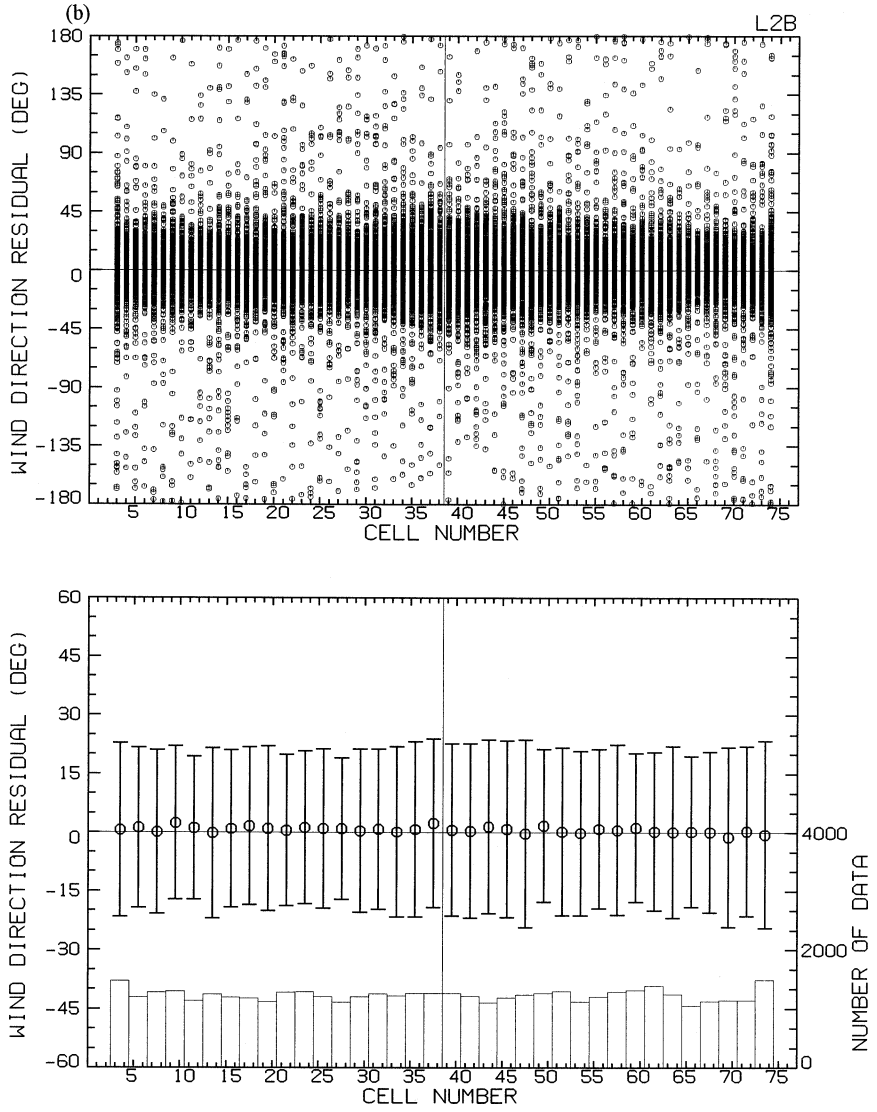

FIG. 6. (*Continued*)

gravity, U_{10N} is the 10-m neutral equivalent wind speed, T_a and T_w are the temperature of air and water in degrees Centigrade, respectively. The inverse wave age, which represents the maturity of wind-wave growth, is calculated as C_p/U_{10N} using U_{10N} and the phase speed of the dominant wave, C_p, is estimated from the buoy wave period through the linear dispersion relation for deep water waves.

In Table 2, the wind speed residual shows low correlation with the parameters representing the thermal condition of the sea surface, such as the sea surface temperature (SST), air–sea temperature difference, and bulk Richardson number, even though the correlation coefficients exceed the 99% confidence level. For example, an increase of 10°C in SST under the same wind condition results in a decrease of wind speed of only -0.23 m s^{-1}. Only the significant wave height (SWH) shows relatively higher correlation with the wind speed residual. An increase of 1 m in SWH causes an increase of wind speed of 0.22 m s^{-1}. This feature does not vary with the wind speed within the range of speeds from 3 to 15 m s^{-1}, where the wind speed residual does not depend on the wind speed. No significant differences among the three wind datasets are also discernible, though the results are not shown here.

In Fig. 7, the wind speed residual (QSCAT-buoy) is plotted against (a) the SST, (b) air–sea temperature difference, (c) SWH, and (d) inverse wave age. Only the data of buoy wind speed ranging from 9 to 12 m s^{-1} are used. Upper panels show scatterplots with linear regression lines, and lower panels show the number of data points, binned averages, and standard deviations, and the linear regression lines. It is shown that the wind speed residuals show weak dependencies on the SWH

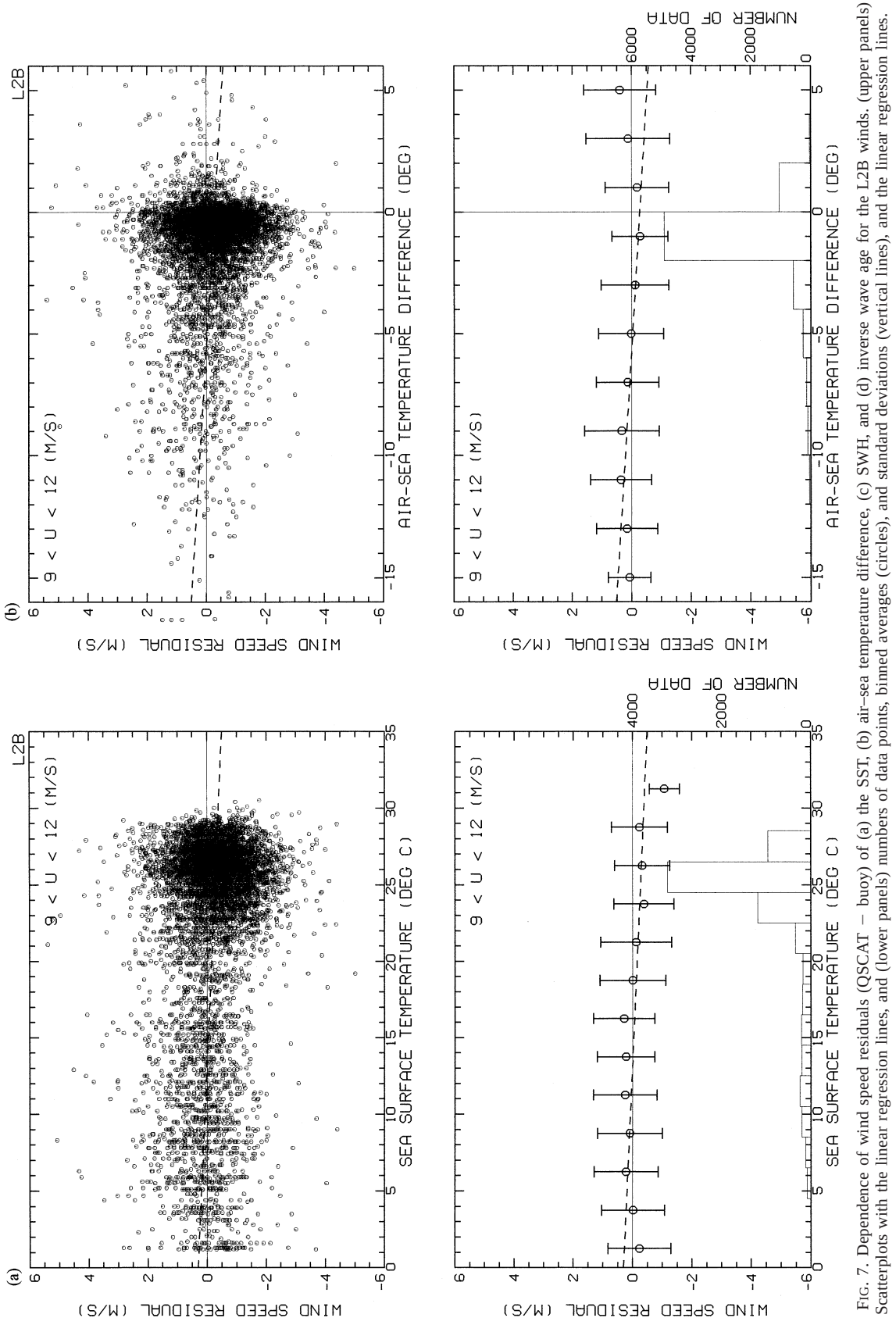

FIG. 7. Dependence of wind speed residuals (QSCAT − buoy) of (a) the SST, (b) air–sea temperature difference, (c) SWH, and (d) inverse wave age for the L2B winds. (upper panels) Scatterplots with the linear regression lines, and (lower panels) numbers of data points, binned averages (circles), and standard deviations (vertical lines), and the linear regression lines.

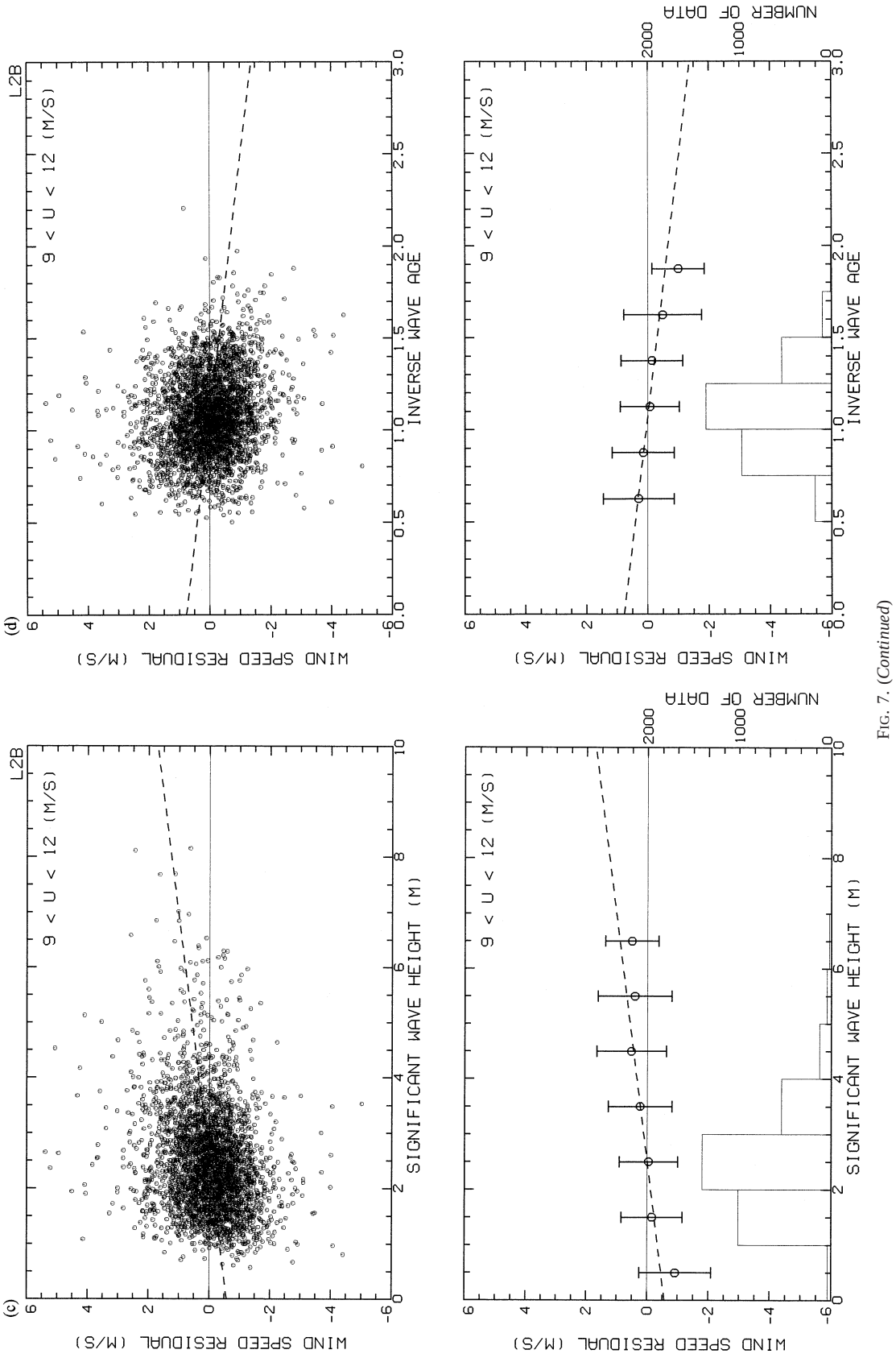

FIG. 7. (*Continued*)

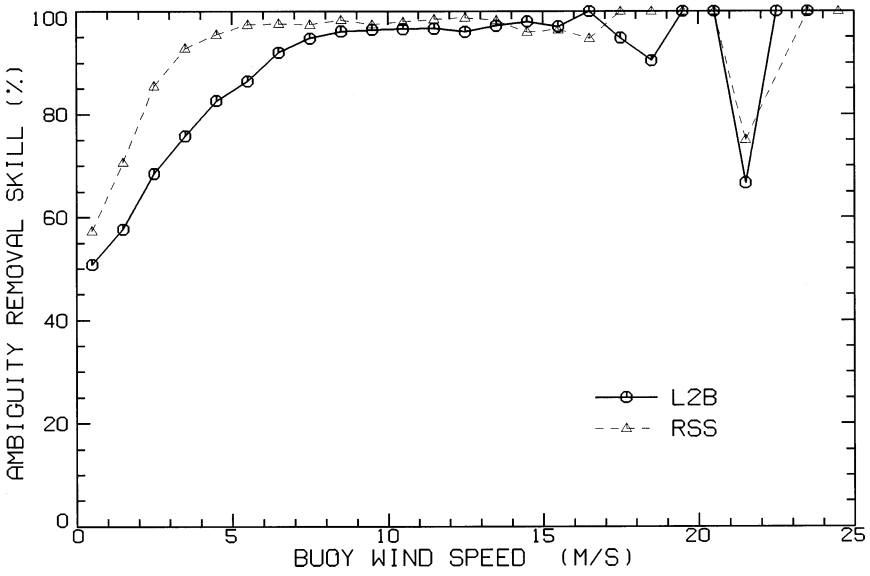

FIG. 8. Skill of the ambiguity removal plotted against the buoy wind speed for the L2B (thick line and circles) and RSS wind data (thin dashed line and triangles).

and inverse wave age, while the SST and air–sea temperature differences are less correlated. These results imply that higher and older dominant wind waves may cause enhanced radar backscattering under the same wind conditions.

One might suspect that one reason why the correlations are so low is the neglect of the effects of ocean currents. Dickinson et al. (2001) and Kelly et al. (2001) demonstrated the effects of the surface current on the vector wind measurements by scatterometers in the Tropical Pacific using the TAO buoy data, since the scatterometers measure the motion of the air relative to the ocean. The influence of the surface current may smear effects of the other parameters. Therefore, we calculated the same correlations using only the NDBC and JMA buoy data, which are considered to be less affected by surface currents. Though the results are not shown here, the correlation coefficients of the wind speed residual with SST or air–sea temperature difference are of the same magnitude or less.

Several previous studies have reported that the microwave backscattering from the sea surface may be influenced by the sea surface temperature (e.g., Donelan and Pierson 1987), the stability of the atmospheric boundary layer (e.g., Keller et al. 1985; Colton et al. 1995), and the sea state (e.g., Keller et al. 1985; Li et al. 1989). By comparing wind vectors derived from the *ERS-1* C-band scatterometer with buoy observations, Ebuchi et al. (1996) and Graber et al. (1996) showed that the wind speed residual shows a negative correlation with the sea surface temperature and a positive correlation with the significant wave height. The sea surface temperature dependence of the scatterometry was confirmed by combining backscattering cross sections observed by the *ERS-1* scatterometer with wind and temperature data derived from European Centre for Medium-Range Weather Forecasts analyses (Ebuchi 1997). However, Ebuchi et al. (1998) reported the wind speed residuals of NSCAT do not show high correlation with the buoy SST, which is consistent with the result of present study. The difference of the microwave frequency might be the reason for the different dependence on the SST.

The stability of the atmospheric boundary layer above the sea surface is considered to have two possible effects. Under the same wind speed at a height above the sea surface (e.g., 10 m), the wind stress (or momentum transfer from the air to water), which generates small-scale waves contributing to the radar backscatter, varies with the atmospheric stability. Under the same wind stress acting on the sea surface, generation of the small-scale waves may also be affected by the stability. The former effect is already taken into account in the present comparison, since the buoy wind speed is converted to the 10-m neutral equivalent wind, which has one-to-one relationship with the wind stress. The latter effect is suggested to be smaller, since it does not appear in the correlation listed in Table 2.

Results of the present study for the QSCAT/SeaWinds Ku-band scatterometer (Table 2) imply that the influence of the thermal condition of the sea surface on the Ku-band radar backscattering is not physically significant. Only the effect of the sea state is represented by the relatively higher correlations of the wind speed residual with the significant wave height and inverse wave age. This conclusion is consistent with results from NSCAT (Ebuchi et al. 1998, 1999), and is considered to represent the nature of Ku-band radar backscatter from the sea surface.

d. Skill of ambiguity removal

When wind vectors are retrieved from backscattering measurements using the MLE algorithm, the MLE gives up to four initial wind vector solutions (''ambiguous'' vectors). Ambiguity removal is a procedure of selecting a unique solution from these ambiguous vectors. The ambiguity removal algorithm for the L2B and RSS data processing is based on a modified median filter technique (Shaffer et al. 1991), with initialization using wind data from the NWP model of the National Centers for Environmental Prediction. The DIRTH algorithm gives a unique solution and does not output ambiguous wind vectors.

In order to assess the completeness of the ambiguity removal procedure, the wind vector selected by the ambiguity removal was compared with the vector closest to the collocated buoy wind vector at each wind vector cell. The skill of the ambiguity removal procedure is defined as the percentage of agreement between the vector chosen by the procedure and that closest to the buoy observation. In Fig. 8, the skill is shown as a function of the buoy wind speed in bins of 1 m s^{-1} for the L2B and RSS data.

For both of the wind data, the skill is relatively low at low wind speeds and increases with the wind speed. For wind speeds higher than 6 m s^{-1}, the value of skill is greater than 90%. The RSS data shows higher skill than the L2B data at wind speeds lower than 8 m s^{-1}. This may be partly due to the more strict rain flagging applied for the RSS data.

Several reasons can be expected for the poor skill at low wind speeds. Both the incompleteness of the ambiguity removal algorithm using the median filter technique as well as errors in the geophysical model function at low winds can contribute to the poor skill. The accuracy of buoy wind direction at low wind speeds may also be doubtful and may spuriously reduce the skill.

4. Summary

Wind vectors observed by QuikSCAT/SeaWinds were compared with wind and wave ocean buoy observations. The three QSCAT wind data, the L2B, DIRTH, and RSS winds, were collocated with observations from the NDBC, TAO, and JMA buoys. Only the buoys located offshore were selected. Time difference and spatial separation between the QSCAT and buoy observations were limited to less than 30 min and 25 km, respectively. Wind speed measured by the buoys at various heights above the sea surface was converted to equivalent neutral wind speed at a height of 10 m.

For the wind speed comparison, the rms difference is about 1 m s^{-1}. No systematic biases depending on wind speed or wind vector cell location are discernible except for overestimation at very high wind speeds. For the wind direction comparison, the rms difference is about 20° when only the data with wind speed higher than 3 m s^{-1} are used. It is concluded that the mission requirements for wind speed and direction are satisfied. The skill of the ambiguity removal procedure was also evaluated using the collocated dataset. It was shown that the skill is greater that 90% at wind speeds higher than 6 m s^{-1}, though the skill is lower at low wind speeds.

Effects of oceanographic and atmospheric parameters on the scatterometry were also assessed using the buoy data. Dependencies of wind speed residual on the sea surface temperature or the air–sea temperature difference are not physically significant, while slight positive correlation with the significant wave height is discernible. These results are different from those for the ERS/AMI C-band scatterometer, but are consistent with those for the NSCAT Ku-band scatterometer.

Acknowledgments. The authors gratefully acknowledge funding support by the National Aeronautics and Space Administration and the National Space Developing Agency of Japan. They also appreciate the National Data Buoy Center, the Tropical Ocean Atmosphere Project Office, and the Climate and Marine Department of the Japan Meteorological Agency for providing the buoy data. The QSCAT data products used in the present study are distributed from the NASA/JPL PO.DAAC and Remote Sensing Systems.

REFERENCES

Bentamy, A., Y. Quilfen, P. Queffeulou, and A. Cavanie, 1994: Calibration of the *ERS-1* scatterometer C-band model. IFREMER/Brest, Tech. Rep. DRO/OS-94-01, Brest, France, 72 pp.

Bourassa, M. A., M. H. Freilich, D. M. Legler, W. T. Liu, and J. J. O'Brien, 1997: Wind observations from new satellite and research vessels agree. *Eos, Trans. Amer. Geophys. Union,* **78,** 597.

Colton, M. C., W. J. Plant, W. C. Keller, and G. L. Geernaert, 1995: Tower-based measurements of normalized radar cross-section from Lake Ontario: Evidence of wind stress dependence. *J. Geophys. Res.,* **100,** 8791–8813.

Dickinson, S., K. A. Kelly, M. J. Caruso, and M. J. McPhaden, 2001: Comparisons between the TAO buoy and NASA scatterometer wind vectors. *J. Atmos. Oceanic Tech.,* **18,** 799–806.

Donelan, M. A., and W. J. Pierson, 1987: Radar scattering and equilibrium ranges in wind-generated waves with application to scatterometry. *J. Geophys. Res.,* **92,** 4971–5029.

Ebuchi, N., 1997: Sea surface temperature dependence of C-band radar cross sections observed by *ERS-1*/AMI scatterometer. *J. Adv. Mar. Sci. Tech. Soc.,* **3,** 157–168.

——, H. C. Graber, and R. Vakkayil, 1996: Evaluation of *ERS-1* scatterometer winds with wind and wave ocean buoy observations. Tohoku University Tech. Rep. CAOS 96-1, 69 pp.

——, ——, A. Bentamy, and A. Mukaida, 1998: Evaluation of NSCAT winds with ocean buoy observations. *Proc. Fourth Pacific Ocean Remote Sensing Conf.,* Qingdao, China, Ocean University of Qingdao, 396–400.

——, ——, ——, and ——, 1999: Evaluation of NSCAT winds with ocean buoy observations. *EORC Bull. Tech. Rep.,* **2,** 39–49.

Freilich, M. H., 1997: Validation of vector magnitude datasets: Effects of random component errors. *J. Atmos. Oceanic Technol.,* **14,** 695–703.

——, and R. S. Dunbar, 1999: The accuracy of the NSCAT-1 vector winds: Comparison with NDBC buoys. *J. Geophys. Res.,* **104,** 11 231–11 246.

Freitag, H. P., M. O'Haleck, G. C. Thomas, and M. J. McPhaden, 2001: Calibration procedures and instrumental accuracies for ATLAS wind measurements. NOAA Tech. Memo. OAR PMEL-199, 20 pp. [Available online at http://www.pmel.noaa.gov/tao/proj_over/sensors.shtml.]

Graber, H. C., N. Ebuchi, and R. Vakkayil, 1996: Evaluation of *ERS-1* scatterometer winds with wind and wave ocean buoy observations. University of Miami, Tech. Rep. RSMAS 96-003, 69 pp.

Huddleston, J. N., and B. W. Stiles, 2000: Multidimensional Histogram (MUDH) rain flag product description (Version 2.1). Jet Propulsion Laboratory, Pasadena, CA, 8 pp. [Available online at http://podaac.jpl.nasa.gov/quikscat/qscat_doc.html.]

Jones, W. L., L. C. Schroeder, D. H. Boggs, E. M. Bracalante, R. A. Brown, G. J. Dome, W. J. Pierson, and F. J. Wentz, 1982: The relationship between wind vector and normalized radar cross section used to derive *Seasat-A* satellite scatterometer winds. *J. Geophys. Res.*, **87,** 3318–3336.

JPL, 2001: QuikSCAT science data product user's manual (version 2.0). Jet Propulsion Laboratory Publ. D-18053, Pasadena, CA, 84 pp. [Available online at http://podaac.jpl.nasa.gov/quikscat.]

Keller, W. C., W. J. Pierson, and D. E. Weissman, 1985: The dependence of X band microwave sea return on atmospheric stability and sea state. *J. Geophys. Res.*, **90,** 1019–1029.

Kelly, K. A., S. Dickinson, M. J. McPhaden, and G. C. Johnson, 2001: Ocean currents evident in satellite wind data. *Geophys. Res. Lett.*, **28,** 2469–2472.

Large, W., J. Morzel, and G. B. Crawford, 1995: Accounting for surface wave distortion of the marine wind profile in low-level ocean storms wind measurements. *J. Phys. Oceanogr.*, **25,** 2959–2971.

Li, F., W. Large, W. Shaw, E. J. Walsh, and K. Davidson, 1989: Ocean radar backscattering relationship with near-surface winds: A case study during FASINEX. *J. Phys. Oceanogr.*, **19,** 342–253.

Liu, W. T., and W. Q. Tang, 1996: Equivalent neutral wind. Jet Propulsion Laboratory Publ. 96-19, Pasadena, CA, 8 pp. [Available online at http://airsea-www.jpl.nasa.gov/data.html.]

Long, D. E., and J. M. Mendel, 1991: Identifiability in wind estimation from wind scatterometer measurements. *IEEE Trans. Geosci. Remote Sens.*, **GE-29,** 268–276.

Masuko, H., and Coauthors, 2000: Evaluation of vector winds observed by NSCAT in the seas around Japan. *J. Oceanogr.*, **56,** 495–505.

McPhaden, M. J., 1995: The Tropical Atmosphere Ocean array is completed. *Bull. Amer. Meteor. Soc.*, **76,** 739–741.

Meindl, E. A., and G. D. Hamilton, 1992: Programs of the National Data Buoy Center. *Bull. Amer. Meteor. Soc.*, **73,** 985–993.

Quilfen, Y., and A. Bentamy, 1994: Calibration/validation of *ERS-1* scatterometer precision products. *Proc. IGARSS'94,* Pasadena, USA, IEEE Geoscience and Remote Sensing Society, 945–947.

Shaffer, S. J., R. S. Dunbar, S. V. Hisao, and D. G. Long, 1991: A median-filter-based ambiguity removal algorithm for NSCAT. *IEEE Trans. Geosci. Remote Sens.*, **GE-29,** 167–174.

Toba, Y., N. Iida, H. Kawamura, N. Ebuchi, and I. S. F. Jones, 1990: Wave dependence of sea-surface wind stress. *J. Phys. Oceanogr.*, **20,** 705–721.

WMO/IOC Data Buoy Cooperation Panel, 1996: Guide to moored buoys and other ocean data acquisition systems. Data Buoy Cooperation Panel (DBCP) Tech. Doc. 8, WMO and IOC, 87 pp.

Yueh, S. H., B. Stiles, W.-Y. Tsai, H. Hu, and W. T. Liu, 2001: QuikSCAT geophysical model function for hurricane wind and rain. *Proc. IGARSS 2001,* Sydney, Australia, IEEE Geoscience and Remote Sensing Society, 4 pp.